Control Architectures of Solar-Powered HVAC Systems: A DC-DC Converter's Perspective

Niraja Swaminathan
School of EECS
Oregon State University
Corvallis, Oregon U.S.A.
Niraja.Swaminathan@ieee.org

Bailey Sauter
School of EECS
Oregon State University
Corvallis, Oregon U.S.A.
sauterb@oregonstate.edu

Yue Cao
School of EECS
Oregon State University
Corvallis, Oregon U.S.A.
Yue.Cao@oregonstate.edu

***Abstract*—Solar-powered energy efficient buildings could tie HVAC systems with solar energy and the grid to function together. Such HVAC systems require the grid, batteries, or other energy storage to supply or consume the excess power. This paper presents four different control architectures for solar-powered HVAC systems, focusing on their DC-DC converters. The analysis finds that a higher transformer turns ratio, as within the converter, is required on architectures with a fixed DC bus as opposed to those with a varying DC bus. On the other hand, the varying DC bus architectures require a wider duty ratio range, higher input inductance and output capacitance, a finding compounded due to larger low-power voltage ripples. The results are validated via hardware experimental testing from a 500 W solar simulator (power supply), a front-end current-fed full-bridge DC-DC converter, and a variable load mimicking the HVAC. A table then summarizes the features, advantages, and disadvantages of each architecture.**

***Index Terms*—Energy efficient buildings, HVAC, solar, DC architecture, DC-DC converter, full-bridge converter, energy storage**

I. Introduction

Low-energy and net-zero-energy buildings are increasingly common construction projects. The related design and research is vast and spans many engineering disciplines. Great progress has been made, with the construction and planning of several high-profile buildings. For example, the city of Boston proposed a zoning plan requiring net-zero emissions from all newly constructed large buildings [1]. In electrical engineering, a key element of net-zero design has been on-site renewable power generation, most often from solar panels, to meet the building energy requirement and manage excess power to and from the grid. This solution comes with the typical challenges of solar panels, particularly the variation of panel power. This includes not just nighttime power consumption, but more rapid variations in solar power caused by environmental changes such as clouds, birds, dirt, and more. The variation is mitigated by rapid energy storage used to avoid noticeable interruptions to the building's power supply.

Heating, ventilation, and air conditioning (HVAC) systems make up a large portion (about 50%) of the energy consumed in residential and commercial buildings [2]. Past research in this sub-field has explored a wide range of topics, such as HVAC system modeling and simulation [3], smart frequency control of HVAC drives capable of regulating thermal energy in commercial buildings [4], which has been suggested as a feasible on-site energy storage solution for rapid variations in solar power generation [5], and an entire "next-generation" HVAC system architecture that conserves energy through the temperature variation of water [6].

This paper expands on the aforementioned HVAC research, focusing on potential designs of a solar-powered HVAC system with power electronic converter hardware modification, especially on the solar-tied DC-DC side. To make the control simple and reliable, the solar PV modules are connected to the DC bus through a DC-DC converter, instead of the AC link. The assumption is based on the fact that the conventional HVAC drive, which consists of AC-DC and DC-AC converters, is accessible via several flexible coupling points such as the DC bus for solar penetration. In order to implement an intelligent and energy-efficient design, an overview and evaluation of various design control architectures is presented. Four architecture examples explore the use of both batteries and the grid. The maximum power point tracking (MPPT) control parameter is also varied among architectures. The design of each architecture is presented alongside its advantages, disadvantages, and challenges. Hardware experimental results are obtained with a focus on DC-DC performance evaluating the circuit components and DC bus capacitance requirements.

This paper presents the four different control architectures in Section II, and Section III discusses the analysis of these architectures based on the parameter design and filter requirements. Section IV presents the hardware experimental validation of the analysis and summarizes the key features of the four architectures. Section V concludes the work.

II. Control architectures

For the HVAC system fed from a solar source, another source such as grid and/or battery is necessary to supply or consume the excess power. Based on the fact, this section proposes four architectures for the solar-fed HVAC system and discusses their advantages, difficulties, and feasibility.

A. Architecture-I

Architecture-I consists of an HVAC system with solar and battery sources, as shown in Fig. 1. With this architecture, the DC-DC converter's local feedback controller governs the output voltage. In contrast, the MPPT controller uses V/f control on the inverter to vary the power drawn by the load to operate the system at MPP. Therefore, the MPPT control parameter is the HVAC's line frequency for this architecture.

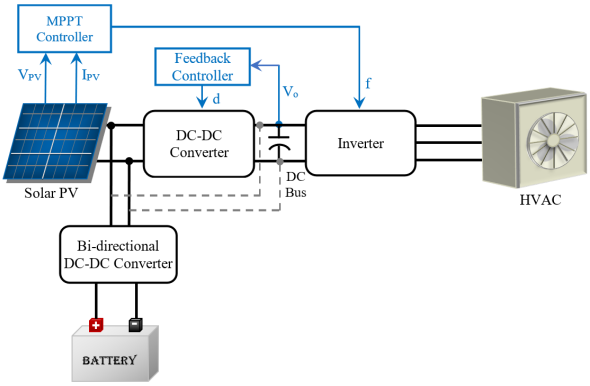

Fig. 1: Architecture-I

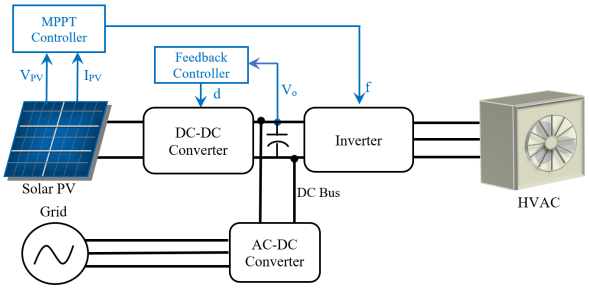

Fig. 2: Architecture-II

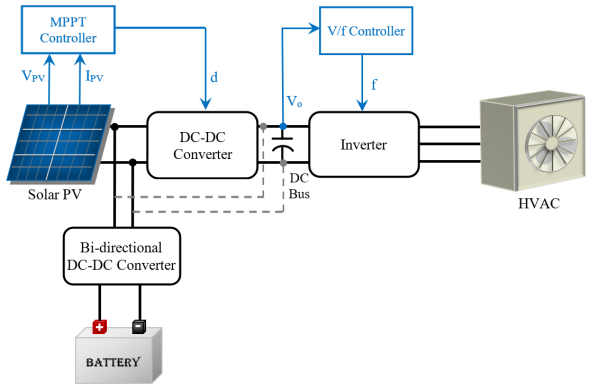

Fig. 3: Architecture-III

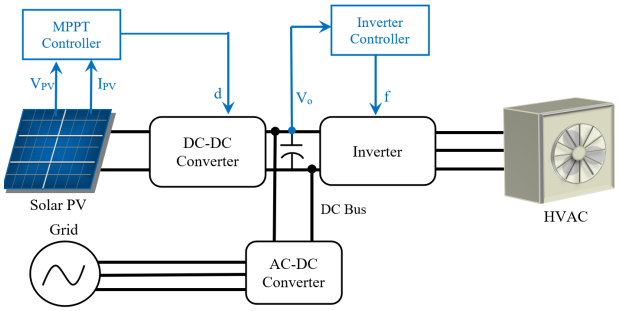

Fig. 4: Architecture-IV

That said, the HVAC motor must be capable of operating in under-frequency conditions. Not only V/f control, but other control techniques, such as direct torque control or field oriented control, could also be used. Additionally, a battery bank is employed, adding to the overall system cost and size. Despite the high cost, this architecture has lower DC bus capacitance requirement due to fixed DC bus voltage, improving the power density.

B. Architecture-II

Architecture-II consists of an HVAC system fed from solar power and the grid, as shown in Fig. 2. The grid is connected directly to the DC bus through an AC-DC converter. This architecture has an option of including the battery; however, this would require an additional bidirectional converter to charge/discharge and increase system cost. Similar to Architecture-I, the DC-DC converter's local feedback controller regulates the output voltage, and the MPPT controller governs the solar PV power using V/f control on the inverter.

C. Architecture-III

Architecture-III, shown in Fig. 3, consists of an HVAC system fed from solar and battery similar to Architecture-I. However, in this architecture, the MPPT controller sets the duty cycle D of the DC-DC converter, making the DC bus voltage variable. Constant flux control (V/f control) of the motor is implemented through the inverter to command the HVAC. According to the available DC bus voltage, the line frequency is adjusted. As a battery bank is necessary to feed the excess load demand, an additional bidirectional DC-DC converter must charge/discharge the battery and the previously mentioned disadvantages of a battery bank are present.

D. Architecture-IV

Architecture-IV, shown in Fig. 4, consists of an HVAC system fed from solar power and the grid similar to Architecture-II. The difference in this architecture is that the MPPT controller sets the duty cycle D of the DC-DC converter, making the DC bus variable. Battery bank is optional for this architecture as the grid can source the excess load demand. However, if a battery bank is employed, an additional bidirectional converter is required. In this architecture, the MPPT controller governs the line frequency through a V/f control on the inverter, similar to Architecture-II. Because the DC bus voltage is variable in this architecture, and can go as low as 120 V from the nominal 380 V voltage, the filter capacitance is burdened.

III. Analysis of Control Architectures

This section presents the analysis, advantages, and limitations of each architecture along with a feasibility study. The architectures with varying DC bus voltages require larger filter capacitance and a wide duty ratio operating range. Therefore, filter capacitance design and duty ratio range are critical to comment on the respective architecture's implementation feasibility.

Table I provides the specification considered for the analysis (STC refers to a solar PV module's standard condition of 1000 W/m^2 and 25°C) but note that the values are scalable depending on the building load.

A current-fed full-bridge (CFFB) converter topology shown in Fig. 5 is chosen for the DC-DC stage due to its: 1) high DC-voltage gain with a lesser transformer turns ratio; 2) non-pulsating input current; and 3) lesser voltage

TABLE I: Specification of the considered system

Specification	Value	Units
MPP voltage at STC	60	V
MPP power at STC	1000	W
DC bus voltage (max)	380	V

stress on the output diodes due to a capacitive filter [7]. This topology is symmetrical-duty controlled with the overlap between the H-bridge leg's top and bottom switches. Therefore, the minimum possible duty ratio is 0.5 (ideally) to ensure uninterrupted current flow through the input inductor L_b. In this topology, the diagonal switches are switched simultaneously. With the above-described switching scheme, the DC voltage gain M, input inductor L_b and output filter capacitor C_f design equations are given in (1), (2) and (3), respectively.

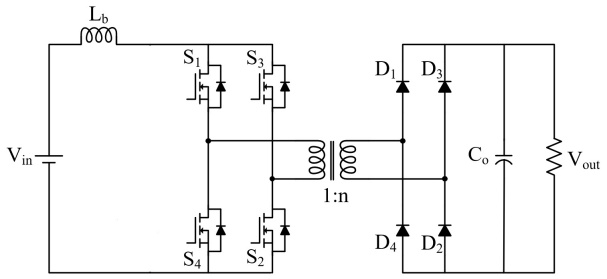

Fig. 5: Current-fed full-bridge (CFFB) converter topology

$$M = \frac{V_o}{V_{in}} = \frac{n}{2(1-D)} \tag{1}$$

$$L_b = \frac{V_{in(min)} * (D - 0.5)}{f_s * \Delta I_{in}} \tag{2}$$

$$C_f = \frac{I_{o(max)} * D}{f_s * \Delta V_o} \tag{3}$$

where V_{in} and V_o are the input and output voltages (V), D is the duty ratio, n is the transformer turns ratio, $I_{o(max)}$ is the maximum output current (A), f_s is the switching frequency (Hz), and ΔV_o is the desired output voltage ripple (V).

Architecture-I and -II have a fixed DC bus voltage, while Architecture-III and -IV have a varying DC bus voltage, as discussed in the previous section. To analyze these architectures, the following design assumptions are considered. The PV power variation is taken to be 10% to 100% of the rated power (at STC condition), so that the respective DC-DC converter output current is between 0.26 A and 2.6 A for the 380 V DC bus. The MPP voltages vary between 50 V and 60 V at different irradiances and temperature conditions for the considered PV array. With these assumptions, the CFFB converter's parameters and filter capacitance are designed as below.

A. Turns ratio and operating duty ratio range

The design of duty ratio and transformer turns ratio is not unique; however, this work presents one possible solution. The operating duty ratio will be smaller at the high input voltage and larger for the low input voltage. Therefore, the design must ensure the operating duty ratio across all the operating input voltages falls within the permissible range. Below subsections present design procedures for the architectures with constant and variable DC voltage buses.

a) Constant DC voltage bus architectures: Assuming the minimum duty ratio of 0.6 to start with (allowing some window to accommodate the losses in the practical case), the transformer turns ratio n for the 380 V fixed DC bus architectures is obtained from (1) as $n = 5$ for a 60 V input. With the calculated transformer turns ratio value, the maximum operating duty ratio at the lower input voltage of 50 V is determined as 0.67. Therefore, the operating duty ratio range for this system is $D_{range} = 0.6 - 0.67$, which is within the permissible range. Minimum duty ratio of 0.6 is considered in this work to start the calculation. However, in some design cases, the duty ratio range will exceed the permissible values, which then can be adjusted by redesigning the parameters around a different minimum duty ratio.

b) Variable DC voltage bus architectures: The variation in the DC bus voltage is required to obtain the operating duty ratio range for the varying DC voltage bus architectures. The DC bus voltage range with the rated voltage (380 V in this case) being the maximum value is determined by calculating the effective load resistance at the DC-DC converter's full load conditions. The load resistance is calculated as 145 Ω at the full load 380 V, 1000 W condition. Therefore, the voltage variation is calculated to be between 120 V and 380 V for 10% to 100% load variations. Assuming the same minimum duty ratio of 0.6 at the lower DC bus voltage (which is 120 V for the considered specification), the transformer turns ratio and the operating duty ratio are calculated from (1) as $n = 1.6$ and $D_{range} = 0.6 - 0.875$.

Based on the above calculation, it is noted that a higher turns ratio is required for the fixed DC bus based architectures. Simultaneously, in the case of the varying DC bus based architectures, the operating duty range is wide, almost utilizing the complete possible range. In practice, the actual operating range will be more than the calculated values due to the presence of non-idealities, for which the feasibility of implementing varying DC bus based architectures can be questionable.

B. Input inductance requirement

Input inductor L_b is calculated based on the maximum duty ratio and current ripple at the full load condition with lower input voltage. The assumed full load current ripple in this work is 10%. The switching frequency is chosen as 150 kHz.

Substituting the minimum input voltage of 50 V (for the considered specification) and the respective calculated duty ratio in (2), the input inductance value is calculated as 28 μH and 62.5 μH for the fixed and variable DC bus voltage architectures, respectively. It is observed that the filter

inductance requirement for the variable DC bus architectures is more than twice as that of the fixed DC bus architectures.

C. Filter capacitor requirement and voltage ripple calculation

The filter capacitance is calculated based on the maximum operating duty ratio and allowable voltage ripple at the full load condition, which is assumed to be 5% for the analysis in this work.

Substituting the maximum duty ratio of 0.67 and 0.875 in the case of fixed and variable DC bus voltage architectures in (3), the filter capacitance values are calculated as 0.916 μF and 1.19 μF, respectively. Therefore, it is observed that the architectures with varying DC bus voltages require 30% more capacitance than with the fixed DC bus voltage.

The difference in the DC bus capacitance will affect the voltage ripple at the light load conditions. Therefore, from the calculated capacitance values, the voltage ripple at the light load condition (10% of full load) is recalculated as 2.2 V and 4.4 V for the fixed and varying DC bus based architectures, respectively. Interestingly, despite high capacitance requirement, the varying DC bus based architectures exhibit higher voltage ripples at the lower power level, leading to a further increase in the capacitance value.

Therefore, to summarize, for the considered system, the fixed DC bus architectures such as Architecture-I and -II are preferred over the variable DC bus architectures such as Architectures-III and -IV, from the perspective of the filter inductance and capacitance requirements.

IV. Hardware Experimental Validation

In this work, a 500 W solar PV system with a front-end CFFB DC-DC converter and a variable load mimicking the HVAC, as shown in Fig. 6, is implemented to validate the architectures' analysis discussed in the previous sections. The converter utilized SiC MOSFETs for switching on the primary side and SiC Diodes for rectification on the secondary side, as shown in Fig. 7. The DC-DC converter was attached to a non-linear solar-simulating power supply for testing. The converter switching signal was provided by a TI Digital Signal Processor at a frequency of 100 kHz.

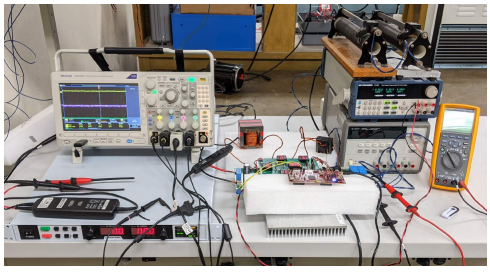

Fig. 6: Experimental setup of 500 W hardware prototype

For Architecture-III and -IV, the MPPT controller varies the DC bus to track MPP. Therefore, understanding the DC bus voltage variation is necessary for the filter capacitor design. Fig. 8 shows the DC bus variation of 190 V to 330 V as the irradiance increases from 350 W/m^2 to 1000 W/m^2 (also shown for both 25°C and 55°C) for the considered

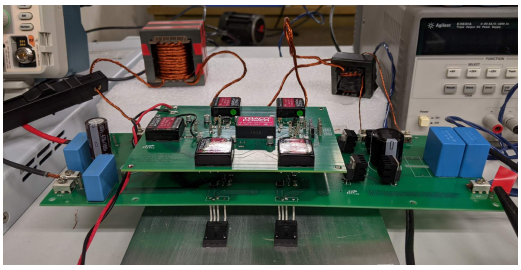

Fig. 7: 500 W DC-DC converter hardware prototype

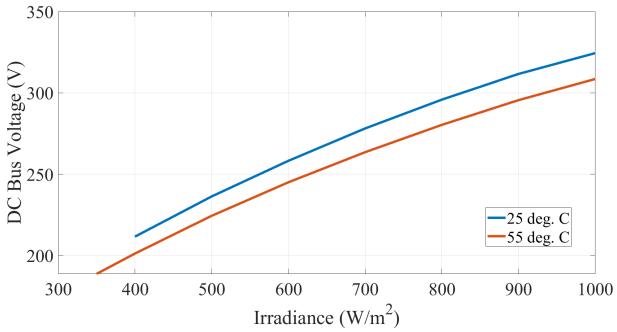

Fig. 8: Experimental results: DC bus voltage variation with changes in load, tested at both 25°C and 55°C

system. The system below 350 W/m^2 is not tested due to the minimum current limitation of the solar simulator and 50% minimum duty limitation of the CFFB converter. The minimum duty shows a limitation of this architecture as the converter was unable to maintain MPP at low irradiance levels. As can be seen, this plot supports the higher capacitance necessity due to the wide DC bus variation range.

The experimental result in Fig. 9(a) shows the input voltage (blue) and current (purple) to the DC-DC converter at standard test conditions at STC (1000 W/m^2 and 25°C). The average voltage and current value of 60 V and 7.3 A verifies the MPP operating condition. Similarly, Fig. 9(b) shows the input voltage and current at 1000 W/m^2 and 55°C. Fig. 10(a) and Fig. 10(b) show the output voltage and current at 25°C with 1000 W/m^2 and 400 W/m^2 irradiance. The output voltage variation of about 120 V is observed between 1000 W/m^2 and 400 W/m^2 irradiance. Therefore, the voltage difference of about 40% puts the burden on the filter requirement in Architecture-III and -IV. Fig. 11 shows the necessary overlapping gating signals (71% duty cycle) characteristic of the CFFB converter architecture. Fig. 12 shows the primary voltage of the transformer (low turns ratio because of variable DC bus).

With respect to the analysis presented in this and previous sections, Table II summarises the key features of the four architectures. Based on whether the grid is available or not, Architecture-I and -II having the fixed DC bus voltage is advantageous and feasible for the implementation due to: a) lower filter inductance and capacitance requirements, b) narrow operating duty range, particularly advantageous when the DC-DC converter exhibits a duty limit, c) simple inverter control due to fixed DC bus voltage, and d) low output voltage ripple at a light load condition.

TABLE II: Features of each architecture

Features	Architectures			
	I	II	III	IV
DC bus voltage	Fixed	Fixed	Variable	Variable
DC bus voltage ripple at light load condition	Small	Small	High	High
Battery requirement	Mandatory	Optional	Mandatory	Optional
Transformer turns ratio	High	High	Low	Low
Filter capacitance	Low	Low	High	High
Operating duty range	Narrow	Narrow	Wide	Wide

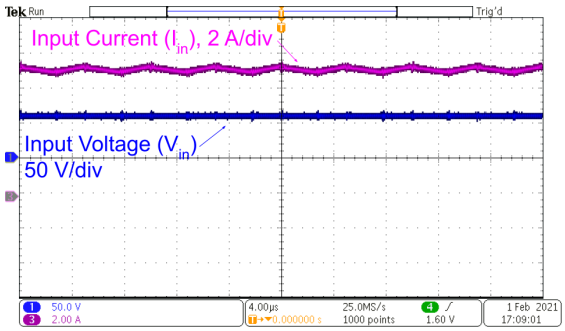

(a)

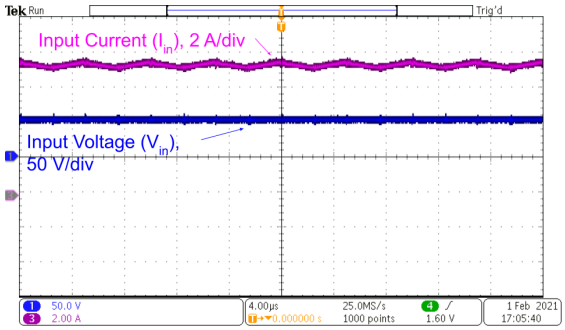

(b)

Fig. 9: Experimental results of DC-DC converter: Input voltage and current at the MPP condition, (a) at 1000 W/m^2 irradiance and 25 $^{\circ}C$, (b) at 1000 W/m^2 irradiance and 55 $^{\circ}C$

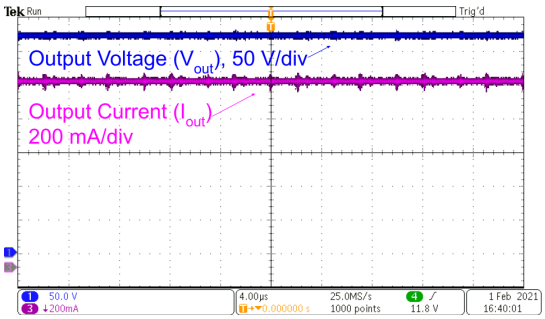

(a)

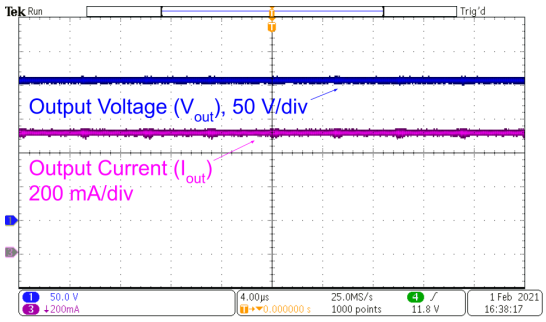

(b)

Fig. 10: Experimental results of DC-DC converter: Output voltage and current at MPP condition, (a) at 1000 W/m^2 irradiance, (b) at 400 W/m^2 irradiance

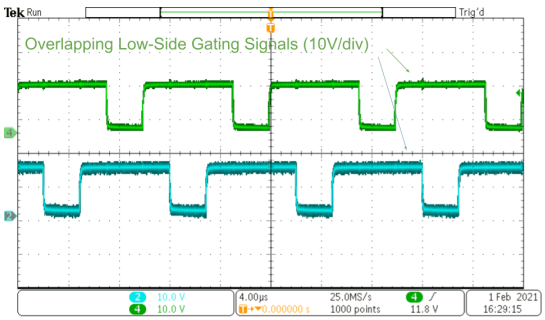

Fig. 11: Experimental results of DC-DC converter: Overlapping PWM gating signals for the low-side MOSFETs

V. Conclusion

This paper presents four control architectures, focusing on DC-DC conversion, of solar-fed HVAC systems considering grid and battery to supply or consume the excess power. Current-fed full bridge DC-DC converter topology is considered for these architectures in this paper. The circuit diagram of this topology and the design equations are presented. This work analyzes the architectures, particularly on the DC bus voltage variations, and their impact on the filter inductance and capacitance requirements and transformer turns ratio. The study reveals that Architecture-I and -II, which have a fixed DC bus voltage, require lesser filter than Architecture-III and -IV with a varying DC bus voltage. For a large solar voltage variation (e.g., 190-330 V as discussed above), the operating duty ratio is also wide if the DC bus is allowed to float, leading to the possibility of the duty exceeding the lower or upper limit. However, the varying DC bus voltage architectures have an advantage on the CFFB transformer turns ratio requirement. The work summarizes these control architectures' advantages and limitations with quantitative results backed up by experimental validations.

References

[1] "Boston zoning change would require net-zero emissions from new buildings,"

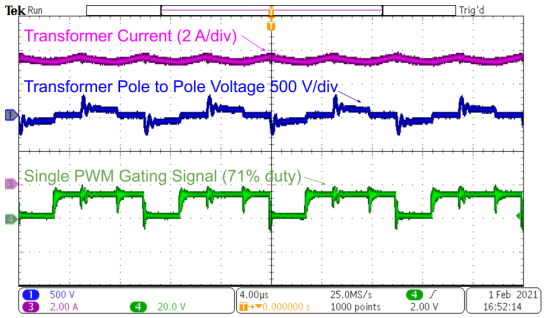

Fig. 12: Experimental results of DC-DC converter: The transformer primary voltage and current, shown with a single MOSFET gate signal from the gate driver

https://energynews.us/2021/01/05/northeast/boston-zoning-change-would-require-net-zero-emissions-from-new-buildings/, accessed: 2021-02-01.

[2] L. Pérez-Lombard, J. Ortiz, and C. Pout, "A review on buildings energy consumption information," *Energy and Buildings*, vol. 40, no. 3, pp. 394–398, 2008. [Online]. Available: https://www.sciencedirect.com/science/article/

[3] C. Szász, "HVAC elements modeling and implementation for net-zero energy building applications," in *2014 IEEE 9th IEEE International Symposium on Applied Computational Intelligence and Informatics (SACI)*, 2014, pp. 195–200.

[4] H. Hao, Y. Lin, A. S. Kowli, P. Barooah, and S. Meyn, "Ancillary Service to the Grid Through Control of Fans in Commercial Building HVAC Systems," *IEEE Transactions on Smart Grid*, vol. 5, no. 4, pp. 2066–2074, 2014.

[5] Y. Cao, J. A. Magerko, T. Navidi, and P. T. Krein, "Power Electronics Implementation of Dynamic Thermal Inertia to Offset Stochastic Solar Resources in Low-Energy Buildings," *IEEE Journal of Emerging and Selected Topics in Power Electronics*, vol. 4, no. 4, pp. 1430–1441, 2016.

[6] Yasuyuki Ito, Yoshiki Murakami, Kenzo Yonezawa, Nobutaka Nishimura, Y. Takagi, Hiroyuki Morimoto, Susumu Sugawara, and Nobuyuki Donen, "Next generation HVAC system," in *2008 SICE Annual Conference*, 2008, pp. 2223–2228.

[7] S. Jalbrzykowski and T. Citko, "Current-Fed Resonant Full-Bridge Boost DC/AC/DC Converter," *IEEE Transactions on Industrial Electronics*, vol. 55, no. 3, pp. 1198–1205, 2008.